nature research

Corresponding author(s): Katrin Andreasson

Reporting Summary

Nature Research wishes to improve the reproducibility of the work that we publish. This form provides structure for consistency and transparency in reporting. For further information on Nature Research policies, see Authors & Referees and the Editorial Policy Checklist.

Statistical parameters

When statistical analyses are reported, confirm that the following items are present in the relevant location (e.g. figure legend, table legend, main text, or Methods section).

n/a	Confirmed	
☐	☒	The exact sample size (*n*) for each experimental group/condition, given as a discrete number and unit of measurement
☐	☒	An indication of whether measurements were taken from distinct samples or whether the same sample was measured repeatedly
☐	☒	The statistical test(s) used AND whether they are one- or two-sided *Only common tests should be described solely by name; describe more complex techniques in the Methods section.*
☐	☒	A description of all covariates tested
☐	☒	A description of any assumptions or corrections, such as tests of normality and adjustment for multiple comparisons
☐	☒	A full description of the statistics including central tendency (e.g. means) or other basic estimates (e.g. regression coefficient) AND variation (e.g. standard deviation) or associated estimates of uncertainty (e.g. confidence intervals)
☐	☒	For null hypothesis testing, the test statistic (e.g. *F*, *t*, *r*) with confidence intervals, effect sizes, degrees of freedom and *P* value noted *Give P values as exact values whenever suitable.*
☐	☒	For Bayesian analysis, information on the choice of priors and Markov chain Monte Carlo settings
☐	☒	For hierarchical and complex designs, identification of the appropriate level for tests and full reporting of outcomes
☐	☒	Estimates of effect sizes (e.g. Cohen's *d*, Pearson's *r*), indicating how they were calculated
☐	☒	Clearly defined error bars *State explicitly what error bars represent (e.g. SD, SE, CI)*

Our web collection on statistics for biologists may be useful.

Software and code

Policy information about availability of computer code

Data collection	Transmission electron microscopy (TEM) images were collected by Gatan Microscopy Suite (GMS) v3
Data analysis	Data was analyzed using GraphPad Prism software (La Jolla, CA); Flow data was analyzed by FlowJo v10 (Ashland, Oregon); TEM images were analzed using ImageJ software v1.6.0_65.

For manuscripts utilizing custom algorithms or software that are central to the research but not yet described in published literature, software must be made available to editors/reviewers upon request. We strongly encourage code deposition in a community repository (e.g. GitHub). See the Nature Research guidelines for submitting code & software for further information.

Data

Policy information about availability of data

All manuscripts must include a data availability statement. This statement should provide the following information, where applicable:

- Accession codes, unique identifiers, or web links for publicly available datasets
- A list of figures that have associated raw data
- A description of any restrictions on data availability

The data that support the findings of this study are available for the corresponding author upon request. Untargeted metabolomics data is available by request to corresponding author.

Field-specific reporting

Please select the best fit for your research. If you are not sure, read the appropriate sections before making your selection.

☒ Life sciences ☐ Behavioural & social sciences ☐ Ecological, evolutionary & environmental sciences

For a reference copy of the document with all sections, see nature.com/authors/policies/ReportingSummary-flat.pdf

Life sciences study design

All studies must disclose on these points even when the disclosure is negative.

Sample size	Sample size was chosen based on power analysis conducted by the "pwr" package from R with effect size of 0.1, alpha < 0.05, and power = 0.8.
Data exclusions	No data was excluded
Replication	Each experiment was repeated three times with a minimum of n = 5 biological replicates, unless otherwise stated. All attempts at replication were successful.
Randomization	This is not relevant to our study as this is not a case/control or clinical study.
Blinding	Investigators were blinded to electron microscopy data when analyzing quantity and quality of the mitochondria between Ido1-/- and WT mouse macrophages, young and old human MDMs, and PTH and veh treated human MDMs.

Reporting for specific materials, systems and methods

Materials & experimental systems

n/a	Involved in the study
☒	☐ Unique biological materials
☐	☒ Antibodies
☒	☐ Eukaryotic cell lines
☒	☐ Palaeontology
☐	☒ Animals and other organisms
☒	☐ Human research participants

Methods

n/a	Involved in the study
☒	☐ ChIP-seq
☐	☒ Flow cytometry
☒	☐ MRI-based neuroimaging

Antibodies

Antibodies used

Anti-Ido1 Abcam 2µg/ml ab55305
Anti-Kmo Abcam 1µg/ml ab130959
Anti-Kynu Abcam 1:1000 ab225916
Anti-3haao Abcam 2µg/ml ab106436
Anti-Human Qprt Abcam 1:1000 ab171944
Anti-Mouse Qprt Sigma-Aldrich 1µg/ml SAB1410425
Anti-Nmnat1 Abcam 1µg/ml ab45652
Anti-NadS Abcam 1:1000 ab45890
Anti-Drp1 BD Transduction Laboratories™ 1:1000 611113
Anti-Fis1 Proteintech 1:1000 10956-1-AP
Anti-LC3BII Cell Signaling Technology 1:1000 3868
Anti-Mff Proteintech 1:1000 17090-1-AP
Anti-Mfn1 Abcam 1:500 ab57602
Anti-Mfn2 Proteintech 1:500 12186-1-AP
Anti-Opa1 Santa Cruz Biotechnology 1:500 sc-393296
Anti-TIM17 Santa Cruz Biotechnology 1:500 sc-271152
Anti-TOM20 Santa Cruz Biotechnology 1:1000 sc-11415
Anti-VDAC Abcam 1:2000 14734
Anti-Sirt3 Cell Signaling Technology 1:1000 C73E3
Anti-Sod2-K68 Abcam 1:1000 ab137037
Anti-Sod2 Abcam 1:1000 ab16956
Anti-Ndufc2 Abcam 1µg/ml ab85359
Anti-COXIV Abcam 1µg/ml ab14744

Anti-PAR Trevigen 1:1000 4335-MC-100
Anti-b-actin Cell Signaling Technology 1:2000 3700

Flow Antibodies:
Formatted: Marker, Channel, Catalog #, Dilution, Clone, Supplier

CD14, APC-Cy7, 557831, 1:50, MϕP9, BD Biosciences
CD64, FITC, 560970, 1:50, 10.1, BD Biosciences
CD206, PE, 566281, 1:50, 19.2, BD Biosciences
CD68, PE-Cy7, 565595, 1:200, Y1/82A, BD Biosciences
CD23, BV421, 338521, 1:50, EBVCS-5, BD Biosciences
CD163, 563889, 555660, 1:50, GHI/61, BD Biosciences
CD86, APC, 555660, 1:50, FUN-1, BD Biosciences
EGR-2, APC, 1706691-82, 1:50, ERONGR2, Invitrogen
CD206, BV711, 141727, 1:50, C068C2, BioLegend
CD301, PE, 145703, 1:50, LOM-14, BioLegend
CD80, BV421, 562611, 1:50, 16-10A1, BD Biosciences
CD86, BV605, 563055, 1:50, GL1, BD Biosciences
I-A/I-E (MHC Class II), PerCPCy5.5, 562363, 1:50, M5/114.15.2, BD Biosciences
CD14, PE-Cy7, 553740, 1:50, rmC5-3 BD Biosciences

Validation

For immunoblotting, antibodies to KP and NAD+ synthetic enzymes were validated using positive controls wherein cDNAs for all enzymes were transfected in HEK cells, lysates serving as positive controls. All antibodies are validated in human tissue according to the manufacturer's website.

Animals and other organisms

Policy information about studies involving animals; ARRIVE guidelines recommended for reporting animal research

Laboratory animals

This study was conducted in accordance with NIH guidelines, and protocols were approved by the Institutional Animal Care and Use Committee at Stanford University. All mice were housed in an environment controlled, pathogen-free barrier facility on a 12 h light/dark cycle, temperature, and humidity, with food and water available ad libitum. IDO1 -/- mice backcrossed onto a C57BL/6J background were obtained from Jackson laboratories (Stock No. 005867, Ido1tm1Alm, original contributor: Andrew Mellor, Medical College Georgia) and IDO1+/- and IDO1+/- mice were intercrossed to generate +/+ and -/- genotypes. QPRT-/- (QPRTKO) mice were obtained from Lexicon Pharmaceuticals (The Woodlands, TX) on a C57BL/6J-129SvEv background.

Wild animals

This study did not involve the use of wild animals

Field-collected samples

This study did not involve the use of Field-collected samples

Flow Cytometry

Plots

Confirm that:

☒ The axis labels state the marker and fluorochrome used (e.g. CD4-FITC).

☒ The axis scales are clearly visible. Include numbers along axes only for bottom left plot of group (a 'group' is an analysis of identical markers).

☒ All plots are contour plots with outliers or pseudocolor plots.

☒ A numerical value for number of cells or percentage (with statistics) is provided.

Methodology

Sample preparation

huMDMs were plated in 10 cm plates at 10 x 106 cells / well and were harvested using 0.25% trypsin-EDTA (Cat. No. 25200056, ThermoFisher Scientific, Pittsburgh, PA) at 37°C. Cells were then washed with FACS buffer (PBS with 2% FCS, 2mM EDTA, and 25mM HEPES), followed by incubation with blocking buffer (5% mouse serum in FACS buffer) for 15 minutes at 4°C. Cells were then stained with the desired antibody combinations for 30 minutes at 4°C. Dead cells were excluded with the addition 0.5 µg/mL propidium iodide. Anti-human antibodies used for flow cytometry of huMDMs (Supplementary Materials, Table 2) and are as follows: CD14 APC-Cy7 (clone MϕP9, BD Biosciences, San Jose, CA), CD64 FITC (Cat. No. 560970, clone 10.1, BD Biosciences), CD206 PE (Cat. No. 566281, clone 19.2, BD Biosciences), CD68 PE-Cy7 (Cat. No. 565595, clone Y1/82A, BD Biosciences), CD23 BV421 (Cat. No. 338521, clone EBVCS-5, BD Biosciences), CD163 563889 (Cat. No. 555660, clone GHI/61, BD Biosciences), CD86 APC (Cat. No. 555660, clone FUN-1, BD Biosciences). For the determination of mitochondrial superoxide by flow cytometry, cells were incubated with MitoSOX (3 uM) (ThermoFisher Scientific) at 37oC for 15 min. The media was then removed and cells were washed with HBSS/Ca/Mg twice. The cells were then collected in Eppendorf tubes using Cellstripper (Cat. No. 25-056-CI, Corning, Corning, NY) for 5 min at 37C. Cells were

	centrifuged at 1000 rpm for 5 min and the cell pellet was resuspended in RPMI supplemented with 3% FBS.
Instrument	BD FACSAria II (BD Biosciences)
Software	Raw FCS files were analyzed with FlowJo software (Treestar, Ashland, OR).
Cell population abundance	CD14+ cells consisted of nearly 95% of the population of cells collected per sample.
Gating strategy	The following controls were used: unstained cells, single-stained cells and dead cells. The cells were gated using forward and side scatter, as well as live/dead staining using DAPI (ThermoFisher Scientific).

☒ Tick this box to confirm that a figure exemplifying the gating strategy is provided in the Supplementary Information.

nature immunology

SUPPLEMENTARY INFORMATION

https://doi.org/10.1038/s41590-018-0255-3

In the format provided by the authors and unedited.

Macrophage de novo NAD$^+$ synthesis specifies immune function in aging and inflammation

Paras S. Minhas[1,2], Ling Liu[3,4], Peter K. Moon[1], Amit U. Joshi[5], Christopher Dove[6], Siddhita Mhatre[1], Kevin Contrepois[7], Qian Wang[1], Brittany A. Lee[7], Michael Coronado[8], Daniel Bernstein[8], Michael P. Snyder[7], Marie Migaud[9], Ravindra Majeti[6], Daria Mochly-Rosen[5], Joshua D. Rabinowitz[3,4] and Katrin I. Andreasson[1,10,11]*

[1]Department of Neurology & Neurological Sciences, Stanford School of Medicine, Stanford, CA, USA. [2]Neurosciences Graduate Program, Stanford University, Stanford, CA, USA. [3]Lewis-Sigler Institute for Integrative Genomics, Princeton University, Princeton, NJ, USA. [4]Department of Chemistry, Princeton University, Princeton, NJ, USA. [5]Department of Chemical and Systems Biology, Stanford University, Stanford, CA, USA. [6]Department of Hematology, Stanford School of Medicine, Stanford, CA, USA. [7]Department of Genetics, Stanford School of Medicine, Stanford, CA, USA. [8]Department of Pediatrics, Stanford School of Medicine, Stanford, CA, USA. [9]Mitchell Cancer Institute, University of South Alabama, Mobile, AL, USA. [10]Stanford Neuroscience Institute, Stanford University, Stanford, CA, USA. [11]Stanford Immunology Program, Stanford University, Stanford, CA, USA.
*e-mail: kandreas@stanford.edu

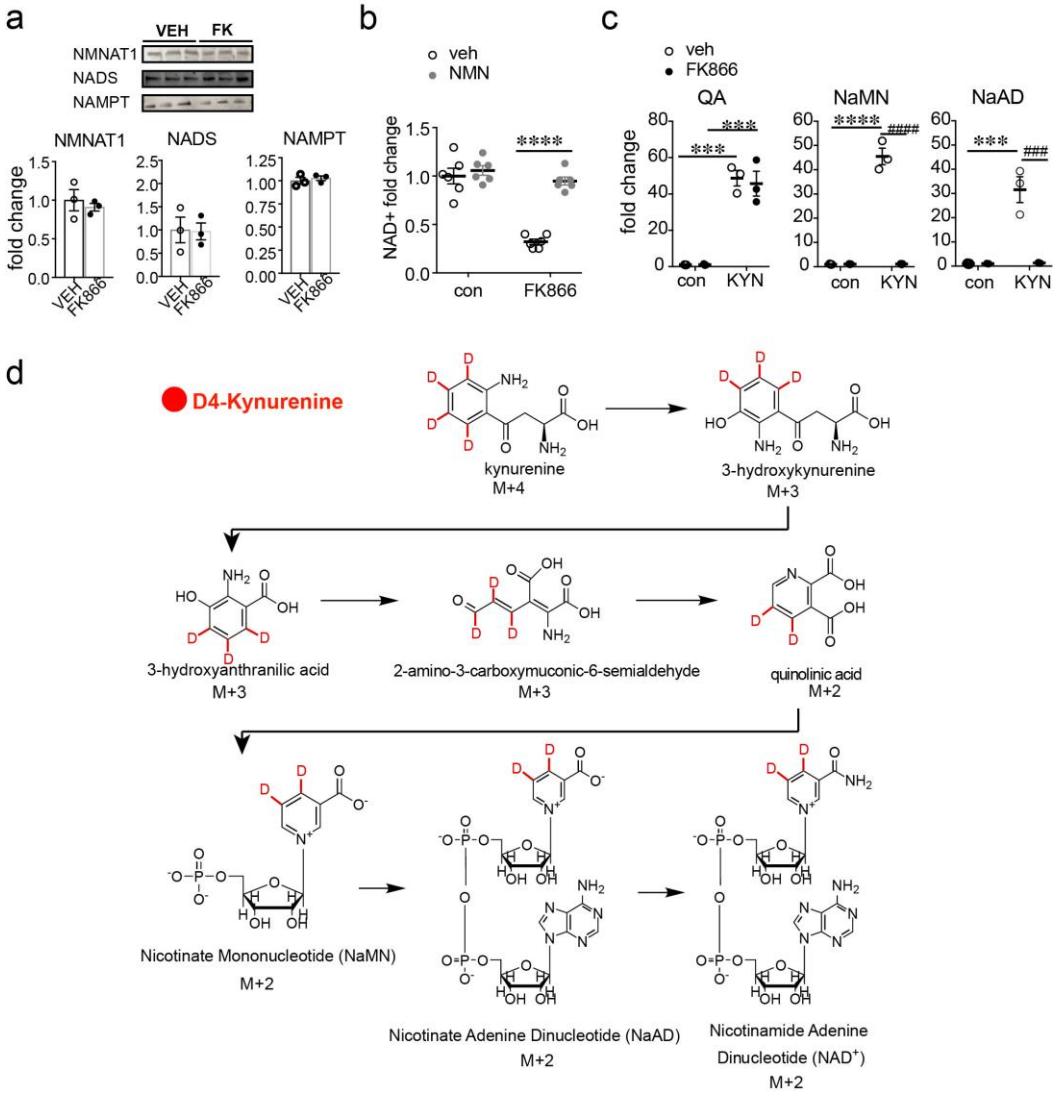

Supplementary Figure 1

Effects of the NAMPT inhibitor FK866 and KYN supplementation.

HuMDMs were treated with either vehicle or FK866 (10 μM, 20 h) and were supplemented with either vehicle or KYN (25 μM, 20 h). **a**, Representative western blot of NAD^+ synthetic enzymes NMNAT1 and NADS and NAMPT; *n* = 3 per group, shown as mean ± S.E. with protein levels normalized to β-actin; non-significance determined by Student's two-tailed *t* test. **b**, Administration of NMN to FK866-treated huMDMs restores NAD^+ levels, as measured by LC/MS; *n* = 6 per group, represented as mean ± S.E., two-way ANOVA: effects of NMN and FK866, $P < 0.0001$ with Tukey post hoc test: ****$P < 0.0001$. **c**, LC/MS measurements of QA, NaMN, NaAD; *n* = 6 per group, represented as mean ± S.E.; two-way ANOVA, for QA effect of KYN, $P < 0.0001$; for NaMN, effects of KYN and FK866, $P < 0.0001$; for NaAD, effects of KYN and FK866, $P < 0.001$; Tukey post hoc tests: ***$P = 0.0001$ QA: veh-veh versus KYN-veh; ***$P = 0.0002$ QA: veh-FK866 versus KYB-FK866; ****$P < 0.0001$ NaMN: veh-veh versus KYN-veh; $^{####}P < 0.0001$ KYN-veh versus KYN-FK866; ***$P = 0.0002$ NaAD: veh-veh versus KYN-veh; $^{###}P = 0.0002$ NaAD: KYN-veh versus KYN-FK866. **d**, Reaction mechanism for isotope labeling of KYN to generate *M*+2 de novo NAD^+**.**

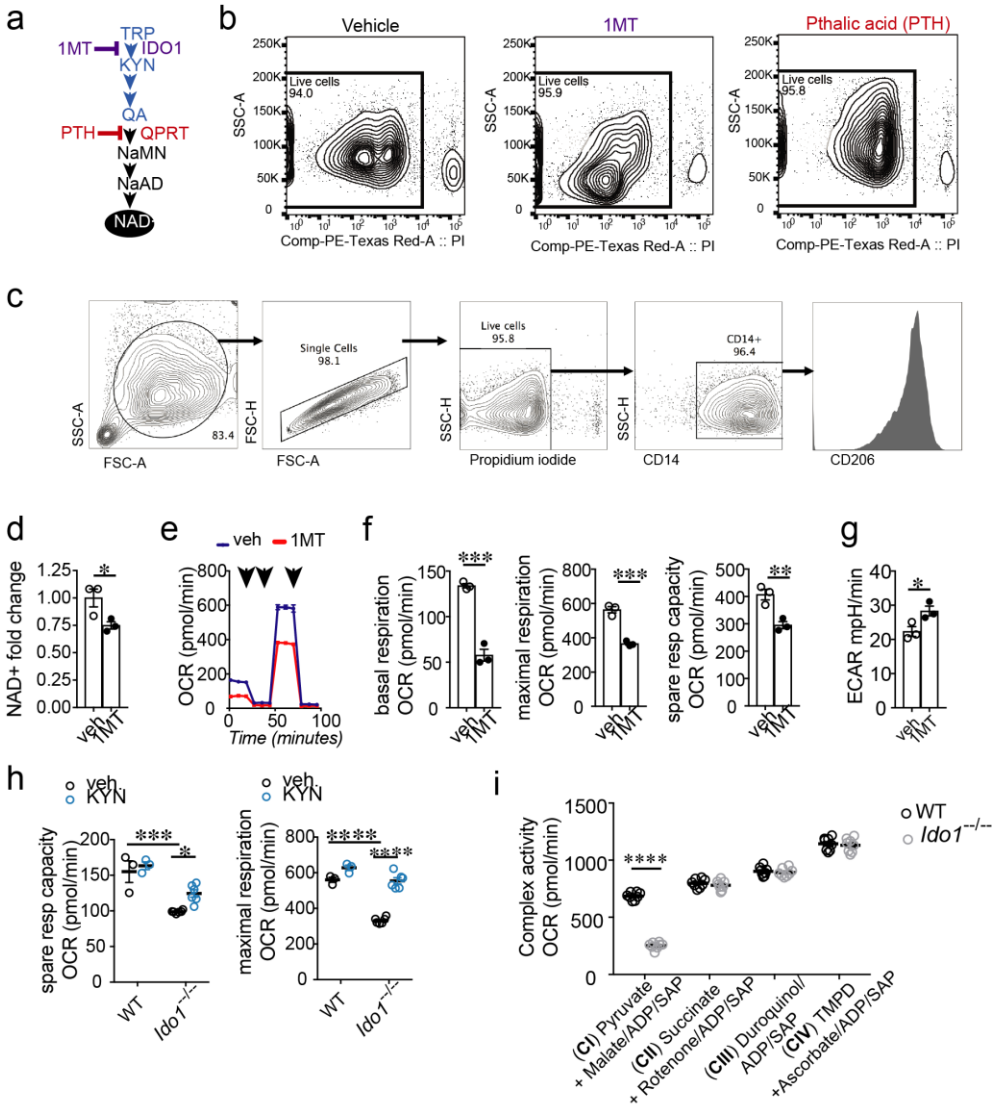

Supplementary Figure 2

Effects of the NAMPT inhibitor FK866 and KYN supplementation.

a, Diagram of the site of action of 1MT and phthalic acid (PTH), selective inhibitors of IDO1 and QPRT, respectively. **b**, Representative flow cytometry plot from three independent experiments of cells treated for 20 h with either vehicle, 1MT (200 μM), or pthalic acid (PTH, 500 μM) stained with propidium iodide (n = 25,000–30,000 cells per group). **c**, Gating strategy for huMDMs. **d–h**, HuMDMs were treated with the IDO1 inhibitor 1MT (200 μM, 20 h). **d**, LC/MS measurement of NAD^+; n = 3 biologically independent samples per group, shown as mean ± S.E.; *P = 0.0233 by Student's two-tailed t test. **e,** Representative trace from three independent experiments for effect of 1MT on OCR, n = 10 biologically independent samples/group, shown mean ± S.E. **f**, Effects of 1MT on basal respiration, maximal respiration, and spare respiratory capacity; n = 3 biologically independent samples per group, shown as mean ± S.E.; ***P = 0.0004 for basal respiration, ***P = 0.0006 for maximal respiration, and **P = 0.0087 for spare respiratory capacity by Student's two-tailed t test. **g**, Effect of 1MT on ECAR; n = 3 biologically independent samples/group, mean ± S.E.; *P = 0.0411 by Student's two-tailed t test. **h**, Peritoneal macrophages from WT and *Ido1*$^{-/-}$ mice were supplemented with either vehicle or 25 μM KYN for 20 h and assayed for spare respiratory capacity and maximal respiration; n = 6 biologically independent samples per WT group and n = 9 biologically independent samples per *Ido1*$^{-/-}$ group, represented as mean ± S.E.; two-way ANOVA, effect of genotype P < 0.0001 for both, effect of KYN P < 0.05 and P < 0.0001 for spare respiratory capacity and max respiration, respectively; Tukey post hoc ***P = 0.0001, *P = 0.0200, and ****P < 0.0001. **i**, Permeabilized macrophages from WT and *Ido1*$^{-/-}$ mice were stimulated with complex-specific substrates, including pyruvate + malate for assessing complex I, succinate + rotenone for complex II, duroquinol for complex III, and TMPD + ascorbate for complex IV. Data are represented as mean ± S.E.; n = 8 biologically independent samples per group; ****P < 0.0001 by Student's two-tailed t test.

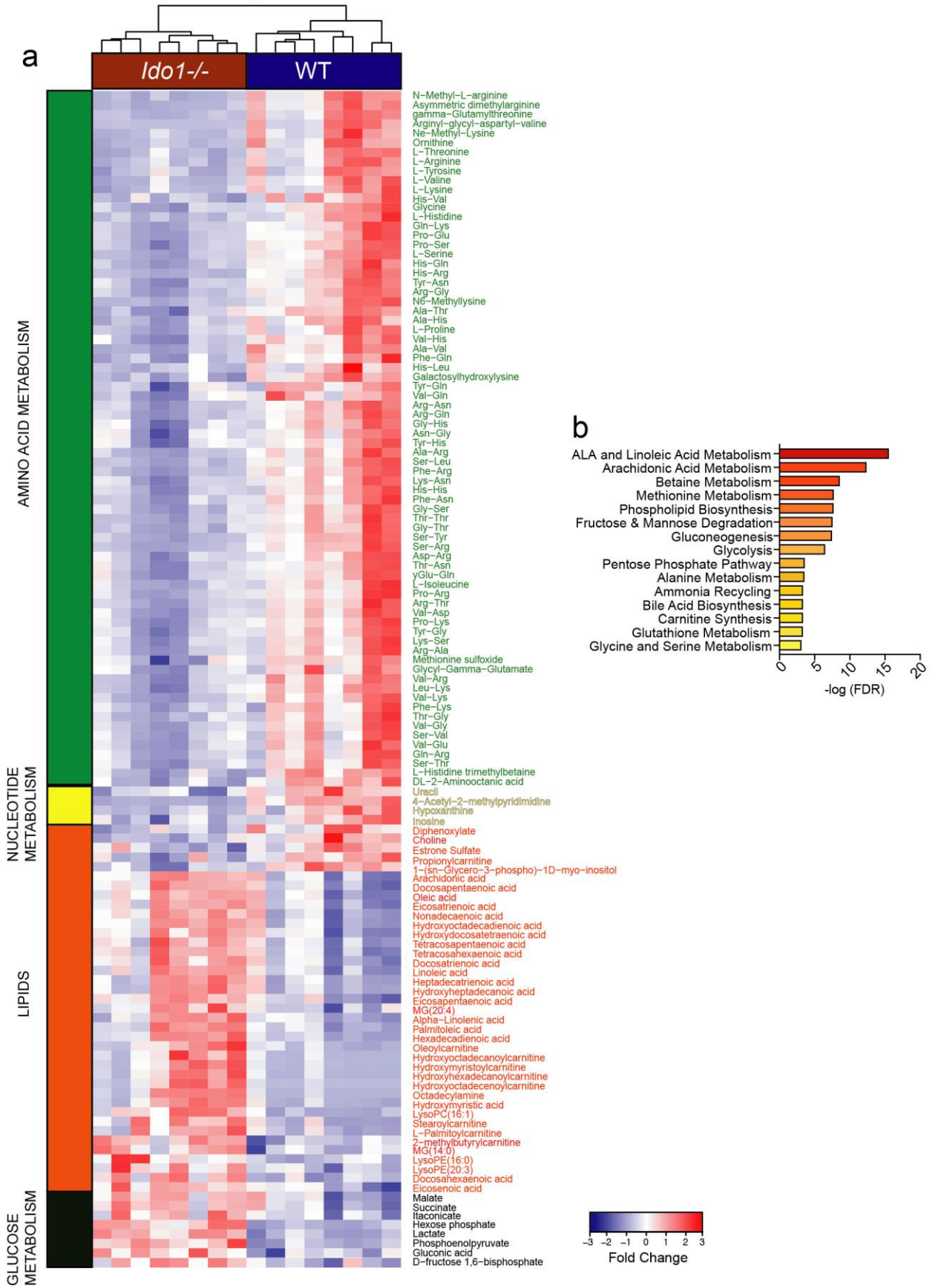
a
Ido1-/-
WT
AMINO ACID METABOLISM
NUCLEOTIDE METABOLISM
LIPIDS
GLUCOSE METABOLISM
N-Methyl-L-arginine
Asymmetric dimethylarginine
gamma-Glutamylthreonine
Arginyl-glycyl-aspartyl-valine
Ne-Methyl-Lysine
Ornithine
L-Threonine
L-Arginine
L-Tyrosine
L-Valine
L-Lysine
His-Val
Glycine
L-Histidine
Gln-Lys
Pro-Glu
Pro-Ser
L-Serine
His-Gln
His-Arg
Tyr-Asn
Arg-Gly
N6-Methyllysine
Ala-Thr
Ala-His
L-Proline
Val-His
Ala-Val
Phe-Gln
His-Leu
Galactosylhydroxylysine
Tyr-Gln
Val-Gln
Arg-Asn
Arg-Gln
Gly-His
Asn-Gly
Tyr-His
Ala-Arg
Ser-Leu
Phe-Arg
Lys-Asn
His-His
Phe-Asn
Gly-Ser
Thr-Thr
Gly-Thr
Ser-Tyr
Ser-Arg
Asp-Arg
Thr-Asn
yGlu-Gln
L-Isoleucine
Pro-Arg
Arg-Thr
Val-Asp
Pro-Lys
Tyr-Gly
Lys-Ser
Arg-Ala
Methionine sulfoxide
Glycyl-Gamma-Glutamate
Val-Arg
Leu-Lys
Val-Lys
Phe-Lys
Thr-Gly
Val-Gly
Ser-Val
Val-Glu
Gln-Arg
Ser-Thr
L-Histidine trimethylbetaine
DL-2-Aminooctanic acid
Uracil
4-Acetyl-2-methylpyridimidine
Hypoxanthine
Inosine
Diphenoxylate
Choline
Estrone Sulfate
Propionylcarnitine
1-(sn-Glycero-3-phospho)-1D-myo-inositol
Arachidonic acid
Docosapentaenoic acid
Oleic acid
Eicosatrienoic acid
Nonadecaenoic acid
Hydroxyoctadecadienoic acid
Hydroxydocosatetraenoic acid
Tetracosapentaenoic acid
Tetracosahexaenoic acid
Docosatrienoic acid
Linoleic acid
Heptadecatrienoic acid
Hydroxyheptadecanoic acid
Eicosapentaenoic acid
MG(20:4)
Alpha-Linolenic acid
Palmitoleic acid
Hexadecadienoic acid
Oleoylcarnitine
Hydroxyoctadecanoylcarnitine
Hydroxymyristoylcarnitine
Hydroxyhexadecanoylcarnitine
Hydroxyoctadecenoylcarnitine
Octadecylamine
Hydroxymyristic acid
LysoPC(16:1)
Stearoylcarnitine
L-Palmitoylcarnitine
2-methylbutyrylcarnitine
MG(14:0)
LysoPE(16:0)
LysoPE(20:3)
Docosahexaenoic acid
Eicosenoic acid
Malate
Succinate
Itaconicate
Hexose phosphate
Lactate
Phosphoenolpyruvate
Gluconic acid
D-fructose 1,6-bisphosphate
−3 −2 −1 0 1 2 3
Fold Change
b
ALA and Linoleic Acid Metabolism
Arachidonic Acid Metabolism
Betaine Metabolism
Methionine Metabolism
Phospholipid Biosynthesis
Fructose & Mannose Degradation
Gluconeogenesis
Glycolysis
Pentose Phosphate Pathway
Alanine Metabolism
Ammonia Recycling
Bile Acid Biosynthesis
Carnitine Synthesis
Glutathione Metabolism
Glycine and Serine Metabolism
0 5 10 15 20
-log (FDR)

Supplementary Figure 3

Untargeted metabolomic profiling of WT and *Ido1*$^{-/-}$ macrophages.

a, Hierarchical clustering of validated and significantly altered metabolites ($q < 0.05$) are represented. *Ido1*$^{-/-}$ macrophages show disrupted amino acid metabolism and lipid metabolism and increased glycolysis ($n = 8$ mice per group, two-tailed parametric Welch's *T*-test with multiple-hypothesis *q*-value correction. FDR < 0.05 was considered significant). **b**, MBROLE enrichment analysis of untargeted metabolomics from comparison of *Ido1*$^{-/-}$ versus WT macrophages ($n = 8$ per genotype).

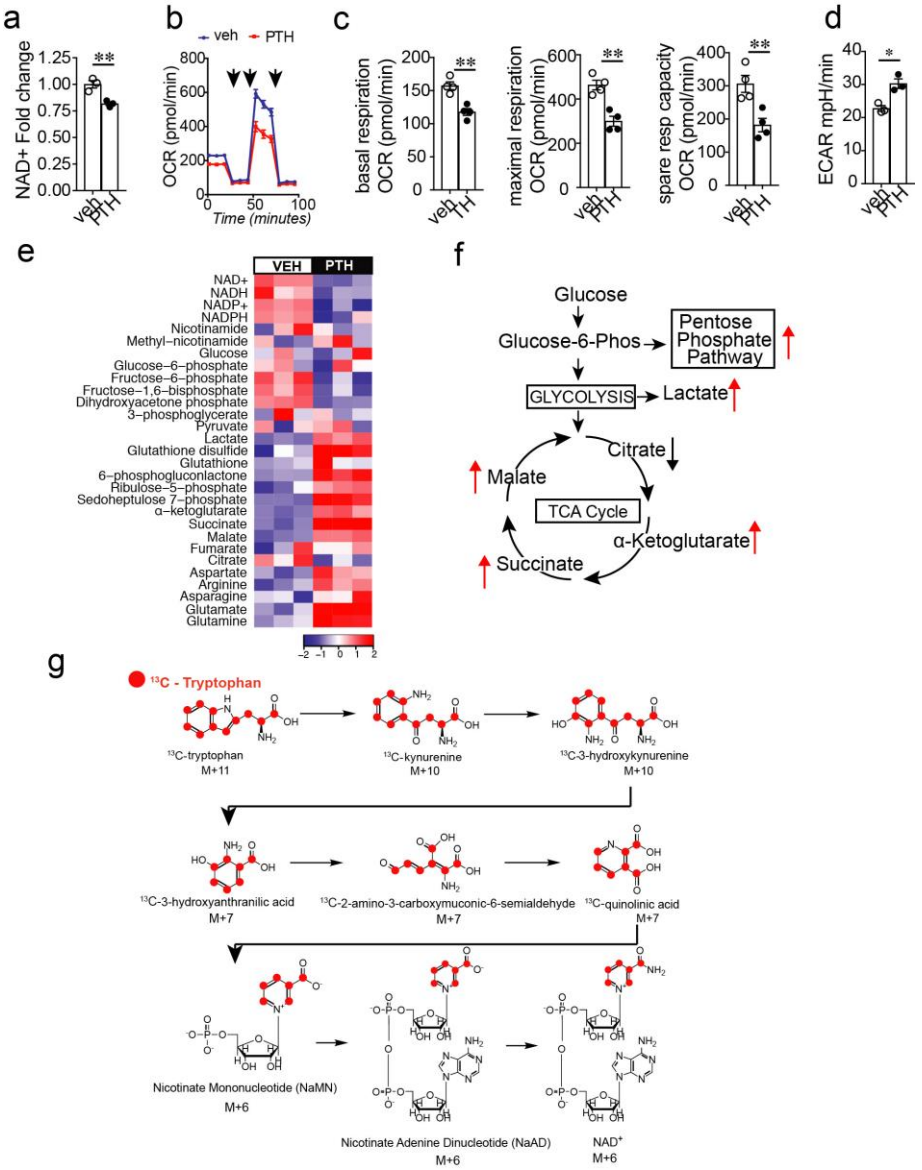

Supplementary Figure 4

Inhibition of QPRT disrupts oxidative phosphorylation and cellular metabolism.

a–**e**, HuMDMs were treated with vehicle or the QPRT inhibitor phthalic acid (PTH; 500 μM, 20 h). **a**, LC/MS of NAD^+ with PTH treatment; *n* = 3 biologically independent samples per group, shown as mean ± S.E.; ***P* = 0.0048 by Student's two-tailed *t* test. **b**, Representative trace of PTH-treated huMDMs. **c**, Basal respiration, maximal respiration, and spare respiratory capacity in PTH-treated huMDMs; *n* = 4 biologically independent samples per group, shown as mean ± S.E; Basal respiration: ***P* = 0.0023; maximal respiration ***P* = 0.0019; spare respiratory capacity: ***P* = 0.0089; all by Student's two-tailed *t* test. **d**, ECAR in PTH-treated huMDMs; *n* = 3 biologically independent samples per group, **P* < 0.05. **e**, Hierarchical clustering of targeted metabolomics for glycolysis, pentose phosphate pathway, and citric acid cycle metabolites of huMDMs treated with PTH (500 μM, 20 h; *n* = 3 biologically independent samples per group). **f**, Targeted metabolomics from **e** with PTH-treated huMDMs reveals an upregulation of lactate, the pentose phosphate pathway and proinflammatory TCA intermediates (in red), similar to changes seen in *Qprt*$^{-/-}$ macrophages. **g**, Metabolism of ^{13}C[TRP] to NAD^+ yields M+6–labeled NAD^+.

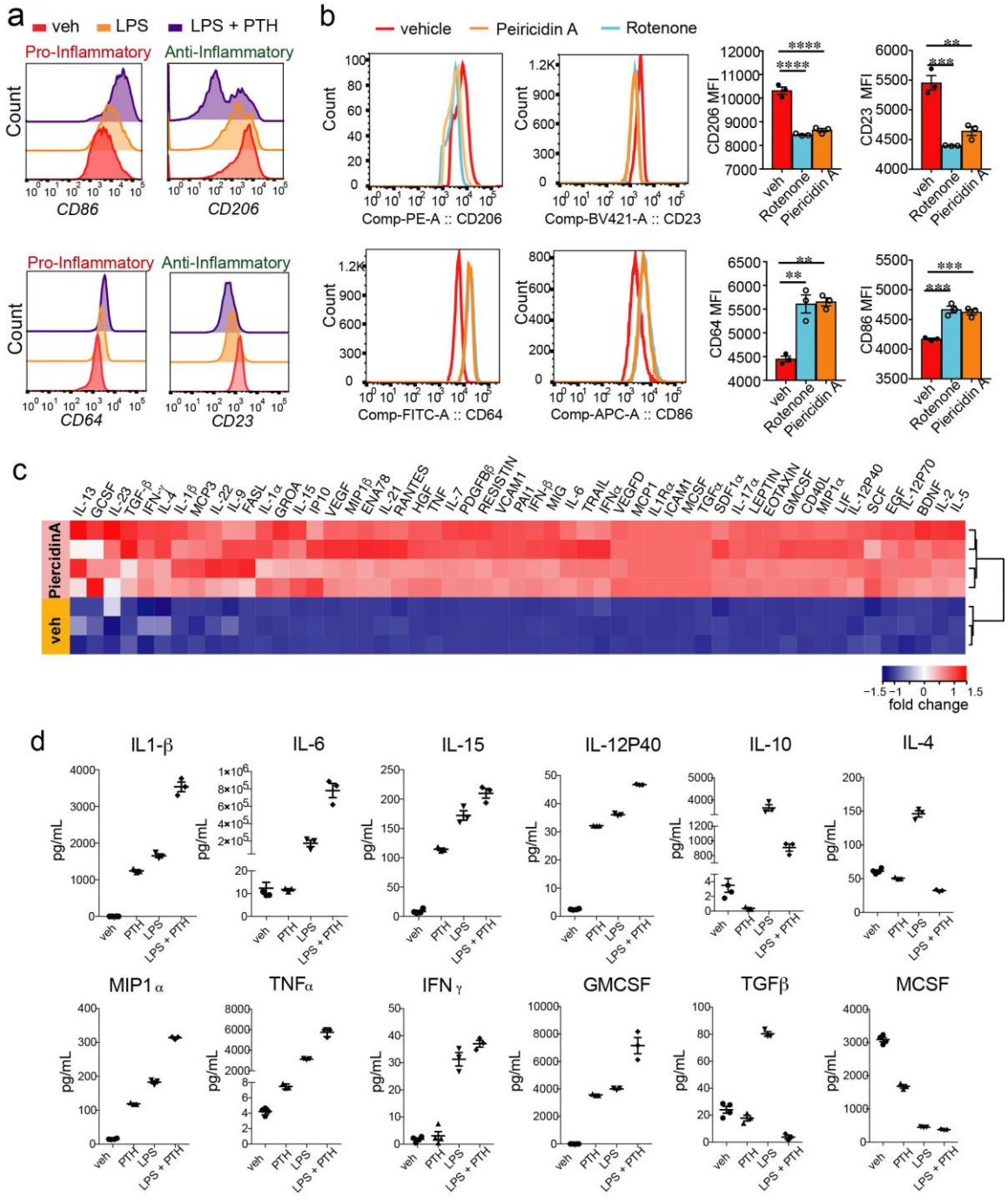

Supplementary Figure 5

Effects of de novo NAD$^+$ synthesis on macrophage polarization.

a, Representative histograms of three independent experiments for surface markers in huMDMs stimulated with LPS and phthalic acid (PTH). **b**, Complex I inhibitors rotenone and piericidin A (500 nM, 20 h) in huMDMs mimic the effect of QPRT inhibition (n = 3 biologically independent samples per group, three independent flow experiments, represented as mean ± S.E.; $^{**}P < 0.01$, $^{***}P < 0.001$. $^{****}P < 0.0001$ by Student's two-tailed t test). **c**, Hierarchical clustering of immune factors in huMDMs treated with either vehicle or piericidin A (500 nM, 20 h). **d**, Quantification of **c**. Significantly regulated immune factors in huMDMs stimulated with PTH and/or LPS, n = 3 biologically independent samples per group, represented as mean ± S.E.

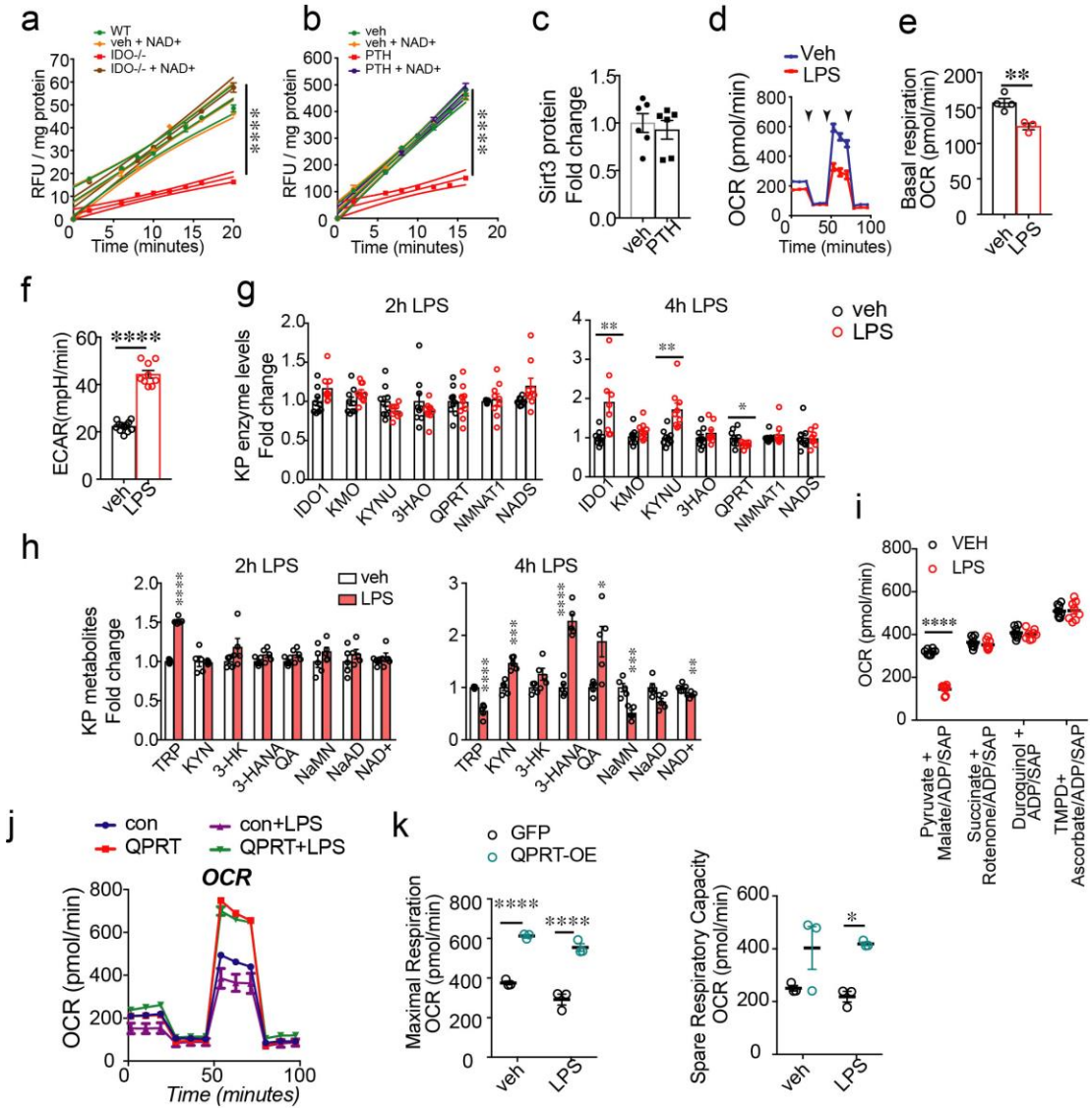

Supplementary Figure 6

Effect of LPS on OXPHOS, the KP, and complex activities.

a, Macrophages from WT and *Ido1*$^{-/-}$ mice supplemented ± NAD^+ (2 mM) and assayed for Sirt3 steady-state kinetics (n = 4 biologically independent samples/group, mean ± S.E.; ****P < 0.0001 by linear regression analysis; curved thin lines denote 95% CI). **b**, Macrophages from huMDMs treated ± phthalic acid (PTH) (500 μM, 20 h) were supplemented ± NAD^+ (2 mM) and assayed for Sirt3 steady-state kinetics (n = 4 biologically independent samples per group, represented as mean ± S.E.; ****P < 0.0001 by linear regression analysis; curved thin lines denote 95% CI). **c**, Quantitative immunoblot of Sirt3 levels in huMDMs ± PTH (500 μM, 20 h), normalized to actin (n = 6 biologically independent samples per group, represented as mean ± S.E.; non-significance determined by Student's two-tailed t test). **d**, OCR trace for huMDMs treated with either LPS (100 ng/mL) or vehicle for 20 h. **e**, Basal respiration in huMDMs following LPS (n = 5 biologically independent samples per veh group, n = 6 biologically independent samples per LPS group, represented as mean ± S.E.; **P < 0.01 by Student's two-tailed t test). **f**, ECAR in huMDMs (n = 9 biologically independent samples/group, mean ± S.E.; ****P < 0.0001 by Student's two-tailed t test). **g**, Changes in KP enzyme levels by quantitative western analysis are observed by 4 h after LPS challenge in huMDMs (n = 8 biologically independent samples per veh group, n = 9 biologically independent samples per LPS group, represented as mean ± S.E.; **P < 0.01 and *P < 0.05 by Student's two-tailed t test). **h**, Increases in KP metabolites are observed by 4 h after LPS challenge in huMDMs (n = 5 biologically independent samples per group, represented as mean ± S.E.; ****P < 0.0001, ***P < 0.001, **P < 0.01, and *P < 0.05 by Student's two-tailed t test). **i**, Permeabilized huMDMs ± LPS (100 ng/mL) were stimulated with complex-specific substrates, including pyruvate + malate for assessing complex I, succinate + rotenone for complex II, duroquinol for complex III, and TMPD + ascorbate for complex IV (n = 8 biologically independent samples per group, represented as mean ± S.E.; ****P < 0.0001 by Student's two-tailed t test). **j**, OCR trace for huMDMs transfected with either GFP control vector or QPRT vector, stimulated with LPS (100 ng/mL) and assayed at 20 h (n = 6 biologically independent samples per

group, represented as mean ± S.E.). **k**, Maximal respiration and spare respiratory capacity of control- and QPRT-transfected huMDMs ± LPS (n = 6 biologically independent samples per group, represented as mean ± S.E.; two-way ANOVA, effect of QPRT $P < 0.0001$ and $P < 0.01$ for maximal respiration and spare respiratory capacity, respectively; effect of LPS $P < 0.01$ for maximal respiration; Tukey post hoc test: *$P < 0.05$, **$P < 0.01$, ****$P < 0.0001$)**.**

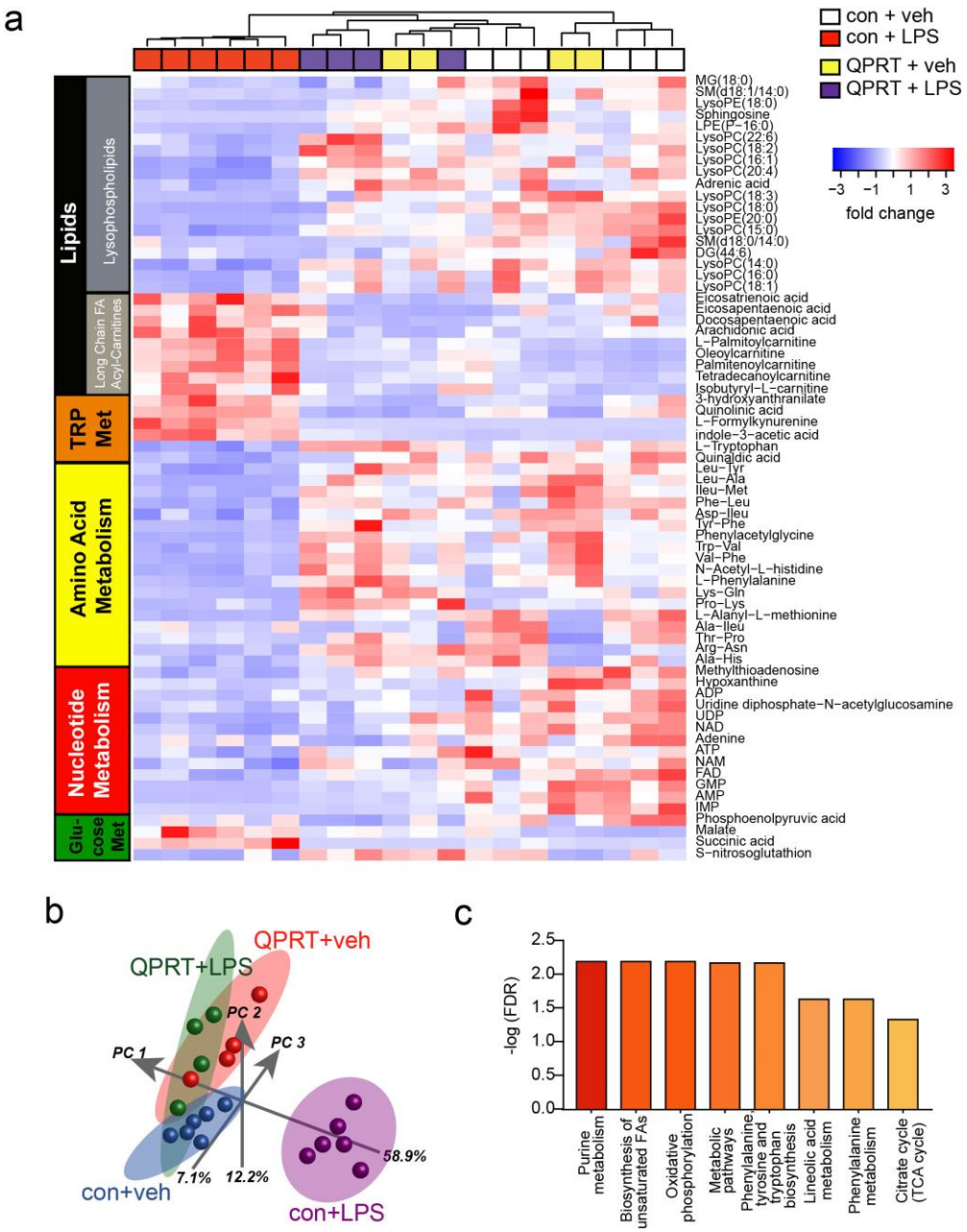

Supplementary Figure 7

Overexpression of QPRT rescues metabolic changes induced by LPS in huMDMs.

Untargeted metabolomics analysis was carried out on huMDMs ± LPS transfected with either GFP control vector or QPRT vector. **a**, Hierarchical clustering of significant validated metabolites is shown ($q < 0.05$ by Student's two-tailed t test with FDR correction for multiple hypotheses; see Methods). Hierarchical clustering reveals rescue of altered amino acid, fatty acid, nucleotide, and glucose metabolism with QPRT overexpression in LPS-stimulated huMDMs ($n = 6$ biologically independent samples per the con + LPS and con + veh groups, $n = 4$ biologically independent samples per group for all others). **b**, Principal-component analysis of **a;** untargeted metabolomics shows separation of LPS-treated control huMDMs from the QPRT + veh, QPRT + LPS, and con + veh groups ($n = 6$ biologically independent samples per the con + LPS and con + veh groups, $n = 4$ biologically independent samples per group for all others). **c**, Enrichment of KEGG pathways ($n = 6$ biologically independent samples per the con + LPS and con + veh groups, $n = 4$ biologically independent samples per group for all others).

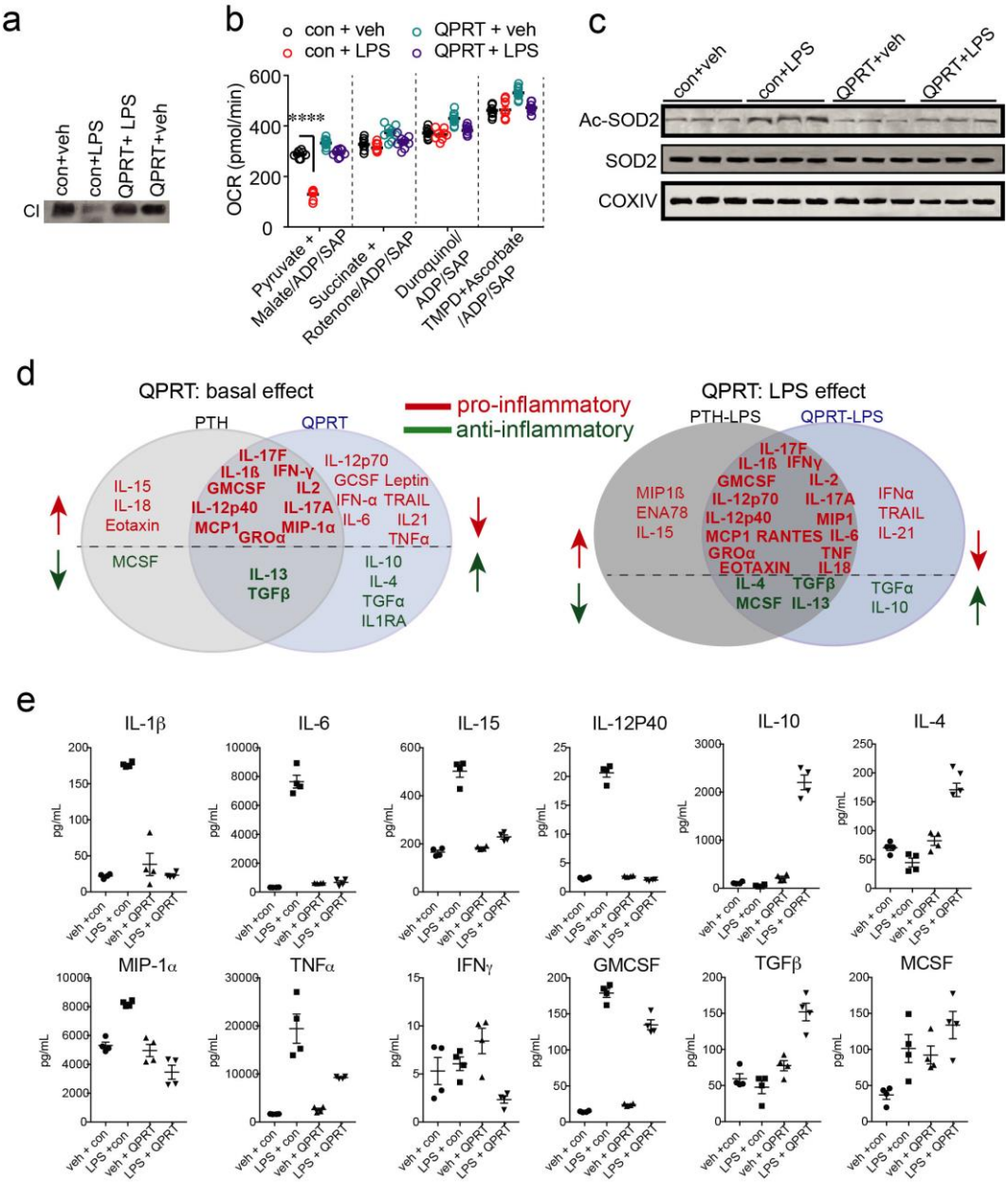

Supplementary Figure 8

Effect of increased de novo NAD$^+$ on immune factor generation in LPS-stimulated macrophages.

HuMDMs transfected with either GFP control vector or QPRT vector were stimulated with LPS for 20 h. **a**, Representative BN-PAGE from three independent experiments. **b**, Permeabilized huMDMs ± LPS were stimulated with complex-specific substrates (n = 8 biologically independent samples per group, represented as mean ± S.E.; ****P < 0.0001 by Student's two-tailed t test). **c**, Representative immunoblot from two independent experiments of SOD2, Ac-SOD2, and COXIV loading control. **d**, Comparison of proinflammatory (in red) and anti-inflammatory (in green) factors that are upregulated and downregulated by QPRT inhibition with phthalic acid (PTH) versus QPRT overexpression under basal conditions (left) and LPS-stimulated conditions (right). Note the similarity of subsets of the pro- and anti-inflammatory factors and reciprocal regulation in control versus experimental conditions. **e**, Representative immune factors regulated by QPRT overexpression in huMDMs ± LPS (n = 3 biologically independent samples per group, represented as mean ± S.E.).

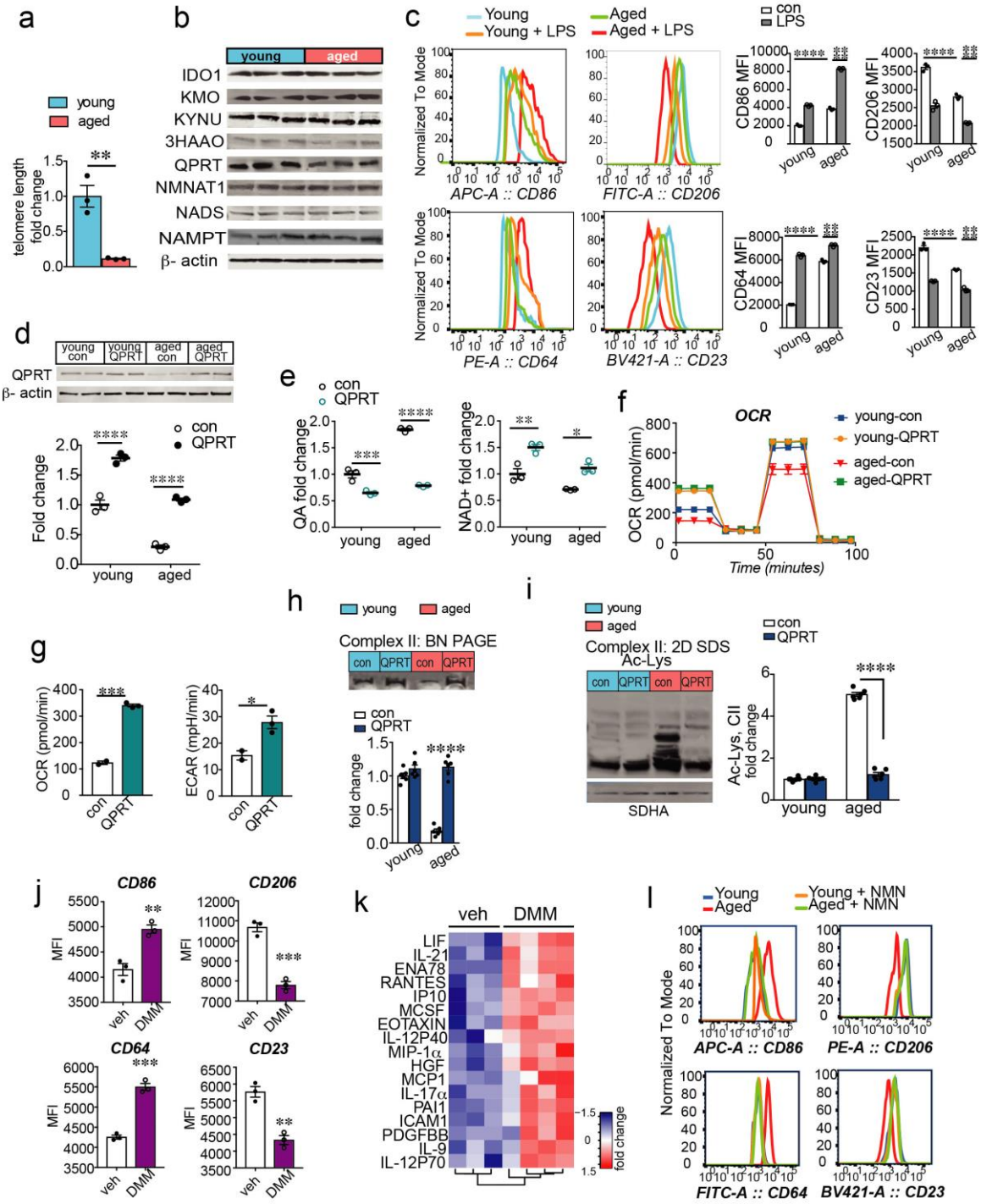

Supplementary Figure 9

De novo NAD$^+$ synthesis regulates mitochondrial respiration and polarization state in aged macrophages.

Young and aged huMDMs were derived from human subjects ≤35 and ≥65 years old, respectively. **a**, qPCR of the telomere length of young versus aged macrophages (*n* = 3 biologically independent samples per group, mean ± S.E.; ***P* = 0.0046 by Student's two-tailed *t* test)**. b**, Representative immunoblots from three independent experiments for all KP enzymes demonstrates loss of QPRT expression in aged macrophages as compared to young macrophages**. c**, Mean fluorescence intensities (MFI) increase for proinflammatory markers CD86 and CD64 and decrease for anti-inflammatory markers CD206 and CD23 in aged versus young huMDMs ± LPS; *n* = 3 biologically independents samples per group, represented as mean ± S.E.; two-way ANOVA: effects of age and LPS, *P* < 0.0001 for all

four surface markers; Tukey post hoc test ****$P < 0.0001$. **d–i**, Young and aged huMDMs were transfected with either control vector (con) or QPRT vector (QPRT). **d**, Top, representative immunoblot from two independent experiments of huMDMs derived from young and aged subjects transfected with control or QPRT vectors. Bottom, quantification of changes in QPRT protein levels; $n = 3$ biologically independent samples/group, mean ± S.E.; two-way ANOVA, effects of age and QPRT $P < 0.0001$; Tukey post hoc test ****$P < 0.0001$. **e**, QPRT overexpression increases metabolism of QA to NAD^+ and restores NAD^+ levels in aged macrophages to those of young huMDMs; $n = 3$ biologically independent samples per group, represented as mean ± S.E.; two-way ANOVA, effect of age and QPRT for QA, $P < 0.0001$; two-way ANOVA, effect of age and QPRT for NAD^+, $P < 0.01$; Tukey post hoc test ****$P < 0.0001$. **f**, OCR trace for young and aged control or QPRT-expressing huMDMs; $n = 3$ biologically independent samples per group, mean ± s.d. **g**, Basal respiration and ECAR in aged control and QPRT-expressing huMDMs; $n = 2$ biologically independent samples per con group, $n = 3$ biologically independent samples per QPRT-OE group, mean ± s.d.; *$P = 0.034$ and ***$P = 0.0001$ by Student's two-tailed t test. **h**, Top, representative BN-PAGE of complex II activity in young and aged huMDMs transfected with either control or QPRT vectors. Bottom, quantification of complex II activity; $n = 6$ biologically independent samples per group, mean ± S.E.; two-way ANOVA, effect of age and QPRT, $P < 0.0001$; Tukey post-hoc test, ****$P < 0.0001$. **i**, Left, representative 2D SDS immunoblot from two independent experiments of complex II in young and aged huMDMs ±, assayed for acetyl-lysine immunoreactivity. Right, quantification of acyl-lysines in complex II; $n = 6$ biologically independent samples/group, mean ± S.E.; two-way ANOVA, effects of age and QPRT, $P < 0.0001$; Tukey post hoc test ****$P < 0.0001$. **j**, MFI of huMDMs treated with the complex II inhibitor dimethyl malonate (DMM, 1 mM, 20 h); $n = 3$ biologically independent samples/group, mean ± S.E.; CD86 **$P = 0.0083$, CD64 ***$P = 0.0003$, CD206 ***P = 0.0005, CD23 **$P = 0.0022$ by Student's two-tailed t test. **k**, Cytokine/chemokine profiles of culture medium from huMDMs stimulated with DMM (1 mM, 20 h). **l**, Representative histograms from three independent experiments of young and aged huMDMs supplemented with NMN (10 μM, 20 h).

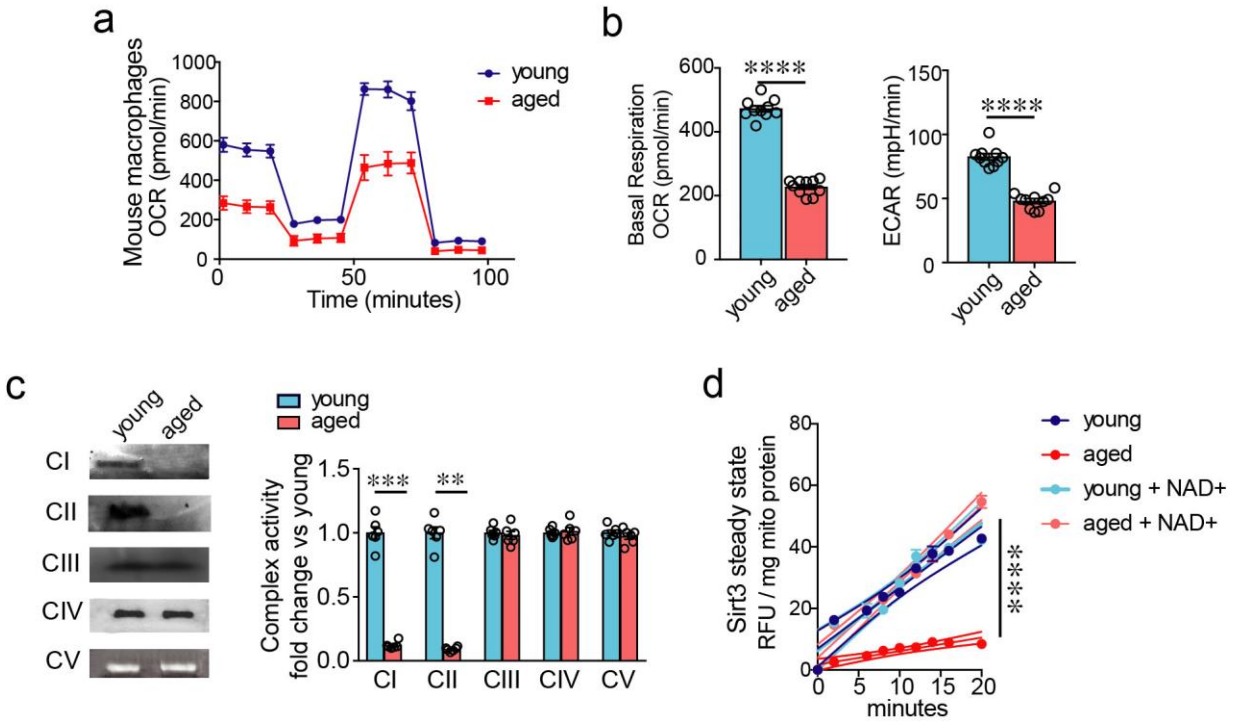

Supplementary Figure 10

Mitochondrial respiration decreases in aged mouse macrophages.

Primary peritoneal macrophages from young (3 month) and aged (16–20 month) mice were examined for mitochondrial respiration, complex activity, and mitochondrial sirtuin steady-state kinetics. **a**, Real-time changes in OCR in young versus aged primary macrophages (n = 10 biologically independent samples per group). **b**, Quantification of basal respiration and extracellular acidification rate (ECAR); n = 10 biologically independent samples per group, represented as mean ± S.E.; ****P < 0.0001 by Student's two-tailed t test. **c**, Left, representative BN-PAGE from three independent experiments of complex activities in young versus aged mouse primary macrophages. Right, quantification demonstrates reduced complex I and complex II activities, n = 6 biologically independent samples per group, represented as mean ± S.E.; ****P < 0.0001 by Student's two-tailed t test. **d**, Young and aged mouse macrophages were assayed for mitochondrial Sirt3 steady-state kinetics; n = 4 biologically independent samples per group, represented as mean ± S.E.; ****P < 0.0001 by linear regression analysis; curved thin lines denote 95% CI.

Supplementary Tables

Supplementary Table 1. Western Blot Antibodies

Antibody	Source	Dilution	Catalog No.
Anti-Ido1	Abcam	2μg/ml	ab55305
Anti-Kmo	Abcam	1μg/ml	ab130959
Anti-Kynu	Abcam	1:1000	ab225916
Anti-3haao	Abcam	2μg/ml	ab106436
Anti-Human Qprt	Abcam	1:1000	ab171944
Anti-Mouse Qprt	Sigma-Aldrich	1μg/ml	SAB1410425
Anti-Nmnat1	Abcam	1μg/ml	ab45652
Anti-NadS	Abcam	1:1000	ab45890
Anti-Drp1	BD Transduction Laboratories™	1:1000	611113
Anti-Fis1	Proteintech	1:1000	10956-1-AP
Anti-LC3BII	Cell Signaling Technology	1:1000	3868
Anti-Mff	Proteintech	1:1000	17090-1-AP
Anti-Mfn1	Abcam	1:500	ab57602
Anti-Mfn2	Proteintech	1:500	12186-1-AP
Anti-Opa1	Santa Cruz Biotechnology	1:500	sc-393296
Anti-TIM17	Santa Cruz Biotechnology	1:500	sc-271152
Anti-TOM20	Santa Cruz Biotechnology	1:1000	sc-11415
Anti-VDAC	Abcam	1:2000	14734
Anti-Sirt3	Cell Signaling Technology	1:1000	C73E3
Anti-Sod2-K68	Abcam	1:1000	ab137037
Anti-Sod2	Abcam	1:1000	ab16956
Anti-Ndufc2	Abcam	1μg/ml	ab85359
Anti-COXIV	Abcam	1μg/ml	ab14744
Anti-PAR	Trevigen	1:1000	4335-MC-100

Anti-β-actin	Cell Signaling Technology	1:2000	3700

Supplementary Table 2. Flow Cytometry Antibodies

Marker	Species Reactivity	Channel	Catalog #	Dilution	Clone	Source
CD14	Human	APC-Cy7	557831	1:50	MφP9	BD Biosciences
CD64	Human	FITC	560970	1:50	10.1	BD Biosciences
CD206	Human	PE	566281	1:50	19.2	BD Biosciences
CD68	Human	PE-Cy7	565595	1:200	Y1/82A	BD Biosciences
CD23	Human	BV421	338521	1:50	EBVCS-5	BD Biosciences
CD163	Human	563889	555660	1:50	GHI/61	BD Biosciences
CD86	Human	APC	555660	1:50	FUN-1	BD Biosciences
EGR-2	Mouse	APC	1706691-82	1:50	ERONGR2	Invitrogen
CD206	Mouse	BV711	141727	1:50	C068C2	BioLegend
CD301	Mouse	PE	145703	1:50	LOM-14	BioLegend
CD80	Mouse	BV421	562611	1:50	16-10A1	BD Biosciences
CD86	Mouse	BV605	563055	1:50	GL1	BD Biosciences
I-A/I-E (MHC Class II)	Mouse	PerCP-Cy5.5	562363	1:50	M5/114.15.2	BD Biosciences
CD14	Mouse	PE-Cy7	553740	1:50	rmC5-3	BD Biosciences

Supplementary Table 3. Electron Transport Chain Complex Substrates

Complex I	2mM Tris-HCl, pH 7.4 0.1 mg/ml NADH 2.5 mg/ml nitrotetrazolium blue
Complex II	4.5mM EDTA 10mM KCN 0.2mM phenazine methasulfate 84mM succinic acid 50mM nitrotetrazolium blue
Complex III	50mM sodium phosphate, pH 7.2 0.5 mg/ml diaminobenzidine
Complex IV	50mM sodium phosphate, pH 7.2 0.5 mg/ml diaminobenzidine 1 mg/ml horse heart cytochrome c
Complex V	35mM Tris 270mM glycine 14mM $MgSO_4$ 0.2% $Pb(NO_3)_2$ 8mM ATP

Supplementary Table 4. Reagents for telomere length PCR

Oligonucleotides	
Telomere FWD: GGTTTTTGAGGGTGAGGGTGAGGGTGAGGGTGAGGGT	Cawthon *Nucleic Acids Res* 2002
Telomere REV: TCCCGACTATCCCTATCCCTATCCCTATCCCTATCCCTA	Cawthon *Nucleic Acids Res* 2002
36B4d FWD: CCCATTCTATCATCAACGGGTACAA	Cawthon *Nucleic Acids Res* 2002
36B4d REV: CAGCAAGTGGGAAGGTGTAATCC	Cawthon *Nucleic Acids Res* 2002

Supplementary Table 5. Vectors for HEK positive controls of KP and NAD-synthesis enzymes

Vectors		
pCMV-A-GFP-tagged plasmid	Origene	PS100026

pCMV-XL5-IDO1-Human Indoleamine-2,3-dioxygeanse plasmid	Origene	SC126221
pCMV-XL5-KMO-Human Kynurenine-3-monoxygenase plasmid	Origene	SC117858
pCMV-AC-KYNU-Human Kynurenine Hydroxylase plasmid	Origene	SC322236
pCMV-HAAO-Human 3-hydroxyanthranilate 3,4-dioxygenase	Origene	SC310572
pCMV-QPRT-Myc-DDK-Human Quinolinate Phosphoribosyltransferase plasmid	Origene	RC202960
pCMV-XL5-NMNAT1-Human Nicotinamide Nucleotide Adenylyltransferase 1 plasmid	Origene	SC122936
pCMV-XL5-NADSYN1-Human NAD Synthetase plasmid	Origene	SC113723